Synchrotron x-ray-scattering study of magnetic-field-induced transitions in Cu$_{1-x}$(Zn, Ni)$_x$GeO$_3$

V. Kiryukhin and B. Keimer

Department of Physics, Princeton University, Princeton, New Jersey 08544

J. P. Hill

Department of Physics, Brookhaven National Laboratory, Upton, New York 11973

S. M. Coad and D. McK. Paul

Department of Physics, University of Warwick, Coventry CV4 7AL, United Kingdom

We have studied the high-field phase behavior of the spin-chain compound Cu$_{1-x}$(Zn, Ni)$_x$GeO$_3$ by synchrotron x-ray scattering in magnetic fields up to 13 T. The rich magnetic phase diagram of this system includes uniform, low-field commensurate spin-Peierls (C), high-field incommensurate spin-Peierls (IC), and Néel phases. For the pure system ($x=0$), we have determined the shape of the phase boundaries as well as the incommensurability and harmonic content of the incommensurate lattice distortion in the IC phase as a function of field and temperature. The results are in good qualitative agreement with predictions based on the soliton lattice model of the IC phase, but significant quantitative discrepancies are found. Dilution of the copper oxide spin-1/2 chains with very small amounts ($x \sim 0.01$) of spin-0 (Zn) or spin-1 (Ni) impurities results in a short-range-ordered IC phase with an anisotropic correlation length comparable to the average impurity separation. This presumably reflects strong pinning of the magnetic solitons to the impurities. For larger x the long-range order is disrupted also in the C phase, and the system undergoes a Néel transition at low temperatures. Aided by supplementary neutron-diffraction measurements, we construct magnetic phase diagrams for the diluted systems. For these systems we also present detailed measurements of the incommensurabilities and correlation lengths as a function of both field and temperature. The data are interpreted in terms of a simple phenomenological model based on lifetime broadening of the spin excitations in finite-sized chain segments. [S0163-1829(96)08934-5]

I. INTRODUCTION

Low-dimensional quantum magnets have long been of interest as prototypical quantum many-body systems. In one dimension, where particularly detailed information about the correlation functions and excitation spectra is available, problems related to interchain coupling and random disorder are currently under intense investigation.

The recently discovered[1] antiferromagnetic spin-chain compound CuGeO$_3$ offers a particularly rich testing ground for theories of these phenomena: The material has a simple structure, and very detailed, quantitative information about the magnetic and lattice vibrational excitation spectra is available. The material contains CuO$_2$ antiferromagnetic chains and allows for the controlled substitution of magnetic and nonmagnetic impurities for the spin-1/2 Cu^{2+} ions through synthesis of the compounds Cu$_{1-x}$(Zn, Ni)$_x$GeO$_3$. The influence of localized impurities on the spin correlations can thus be systematically studied.

The spin chains are coupled through a spin-lattice interaction which arises from the dependence of the intrachain superexchange interaction on the distance between the magnetic atoms. At temperatures below 14.3 K this interaction leads to the formation of a dimerized (spin-Peierls) state[2] whose magnetic signature is a collective singlet state with an energy gap for triplet excitations. The magnetic ground-state

energy in the spin-Peierls state is lowered with respect to the undistorted state. However, neutron-scattering experiments[3] have also revealed a sizable interchain superexchange interaction which favors low-temperature Néel order. Remarkably, the introduction of magnetic and nonmagnetic impurities into the spin chains greatly affects the balance between the two competing interchain interactions and induces a zero-temperature transition from the spin-Peierls state to the Néel state as a function of increasing x.[4–7] The substitution of Si impurities for Ge has a similar effect.[8,9]

In the pure system, the application of a sufficiently high magnetic field has recently been shown to induce a transition from the spin-Peierls phase into an incommensurately modulated phase.[10] This commensurate-incommensurate transition results from a competition between the spin-lattice coupling, which favors the formation of the nonmagnetic spin-Peierls state, and the Zeeman energy, which is minimized for states with a magnetic moment. X-ray[11] and recently also NMR (Ref. 12) experiments have shown that the high-field incommensurate phase has the form of a soliton lattice. Each soliton carries a spin-1/2, and as the field is increased the magnetization increases through continuous proliferation of solitons. The soliton lattice phase persists in the diluted systems, but its long-range order is destroyed.

The interplay between the competing spin-lattice interaction, spin-spin interaction, and Zeeman terms in the Hamil-

tonian results in a rich phase diagram which is the subject of this study. The experimental technique chosen, synchrotron x-ray scattering, lacks dynamic information and is thus complementary to neutron scattering. However, it has two unique advantages for the study of this problem: First, its high momentum resolution allows us to easily resolve the small incommensurability in the modulated phase as well as a small disorder-induced broadening of the Bragg reflections in the diluted systems. Second, the high photon flux enables us to detect satellite reflections 3–4 orders of magnitude less intense than the primary structural superlattice reflections associated with the lattice distortion in the spin-Peierls state. These superlattice reflections are in turn several orders of magnitude less intense than the Bragg reflections characterizing the undistorted lattice. The high photon flux also allows us to study short-range spin-Peierls order in the diluted systems.

The remainder of this article is organized as follows: In Sec. II details of the sample preparation and the experimental setup are given. Section III contains experimental results on the pure system which are compared to extant theoretical predictions. In Sec. IV we present the results of measurements on samples containing controlled amounts of magnetic and nonmagnetic impurities, and a conclusion is given in Sec. V.

II. EXPERIMENTAL DETAILS

Single crystals of $Cu_{1-x}(Zn, Ni)_xGeO_3$ were grown from a CuO-rich flux at Princeton University, and by the floating-zone technique at the University of Warwick. Three crystals grown by the former technique were investigated: $CuGeO_3$, $Cu_{0.985}Zn_{0.015}GeO_3$, and $Cu_{0.98}Ni_{0.02}GeO_3$. These crystals had typical dimensions $0.2 \times 2 \times 2$ mm along the a, b, and c axes, respectively. A large $Cu_{0.97}Ni_{0.03}GeO_3$ crystal of dimensions $3 \times 4 \times 8$ mm grown by the latter technique was also studied. The elemental compositions of the crystals were characterized by electron probe microanalysis. Superconducting quantum interference device magnetometry was used to measure the susceptibility and determine the spin-Peierls transition temperatures of the crystals. These were 14.3, 12.3, 12.0, and ~10 K for the pure, 1.5% Zn-substituted, 2% Ni-substituted, and 3% Ni-substituted crystals, respectively. (As discussed in Sec. IV below, the transition temperature of the $Cu_{0.97}Ni_{0.03}GeO_3$ sample is significantly broadened by disorder.) The measured transition temperatures are in agreement with previous reports.

The x-ray experiments were carried out at beamline X22B of the National Synchrotron Light Source with 8 keV x-rays. The crystals were oriented and loaded into a 13 T split coil vertical field superconducting magnet mounted on a two-circle goniometer. A horizontal axis sample rotator inside the magnet was used for *in situ* adjustments of the sample orientation. Momentum resolutions of 0.005–0.01 Å^{-1} (full width at half maximum) both parallel and perpendicular to the scattering plane were determined by slits before and after the sample in conjunction with the sample mosaicity. The data were collected in a two circle mode near the (3.5, 1, 2.5) superlattice reflection, with momentum transfers of the form $\mathbf{Q}=(3.5K, K, L)$ in the (horizontal) scattering plane. [Momentum transfers are quoted in reciprocal-lattice units

(r.l.u.), that is in units of the reciprocal-lattice vectors $a^*=1.31$ Å^{-1}, $b^*=0.74$ Å^{-1}, $c^*=2.14$ Å^{-1}.] The (3.5, 1, 2.5) reflection is one of the brightest superlattice reflections accessible with our experimental setup. Since the (3.5, 1, 0) direction deviates only 9° from the a axis, the magnetic field is applied almost along the b axis in this scattering geometry, where the critical field is minimum. The value determined from our data at low temperatures, $H_c=12.1$ T, agrees well with susceptibility measurements in this direction.[13]

The neutron-scattering measurements were performed on the H4M triple-axis spectrometer at the High Flux Beam Reactor at the Brookhaven National Laboratory in a pumped helium cryostat. The (002) reflection of pyrolytic graphite (PG) was used as the monochromator and the analyzer, the beam collimations were 40′-40′-80′-80′, and the final neutron energy was 14.7 meV. A PG filter was placed behind the sample in order to eliminate higher-order contamination of the scattered beam. The data were collected in a two-circle mode in the b^*-c^* scattering plane.

III. PURE $CuGeO_3$

$CuGeO_3$ has an orthorhombic structure and contains copper oxide spin chains extending in the c direction. Each copper ion carries spin 1/2 and is octahedrally coordinated to the neighboring oxygens, thereby forming a CuO_4 chain.[14] The nearest-neighbor anti-ferromagnetic superexchange obtained by fitting inelastic neutron-scattering data to a des Cloiseaux-Pearson dispersion is $J_c=10.4$ meV. The same data have also been analyzed in terms of a model which includes next-nearest-neighbor exchange interactions,[15] resulting in $J_{c1} \sim 13$ meV and $J_{c2} \sim 4$ meV. This model reproduces both the magnon dispersions and the temperature dependence of the uniform susceptibility. The exchange constants perpendicular to the spin chains are much smaller ($J_a \sim 0.1 J_c$, $J_b \sim -0.01 J_c$).[3]

Pure $CuGeO_3$ undergoes a spin-Peierls transition at 14.3 K. At the spin-Peierls transition the periodicity of the CuO_2 spin chains doubles. As a consequence, structural superlattice reflections at the commensurate positions ($H/2, K, L/2$), K odd, are observed below the transition temperature in diffraction experiments.[14] Figure 1 shows scans through the (3.5, 1, 2.5) reflection of pure $CuGeO_3$ in the spin-chain direction. In magnetic fields up to ~12 T a single diffraction peak corresponding to the lattice dimerization is observed. In higher fields the peak splits, and its position is then incommensurate with the underlying lattice and is controlled solely by the applied field. The lattice modulation wave vector is only slightly different from its zero-field value, and hence the corresponding diffraction peaks are observed in the vicinity of the zero-field superlattice reflections. As previously observed,[10] the transition is very sharp, and C and IC reflections coexist over a narrow field range, signaling a first-order transition. The data of Fig. 1 were taken at low temperature ($T=4$ K). No significant changes were observed below this temperature. As discussed further below, we have constructed a magnetic phase diagram for $CuGeO_3$ consisting of commensurate (C), incommensurate (IC), and uniform (U) phases, by repeating these scans at higher temperatures. A schematic of this diagram is shown in Fig. 2(a).

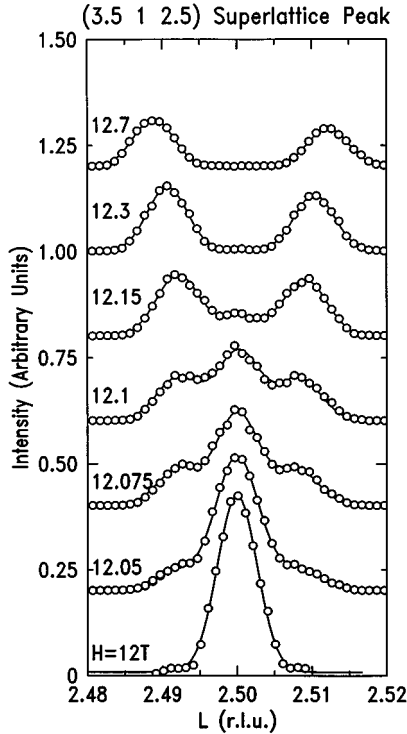In order to determine the harmonic content of the lattice

FIG. 1. Scans through the (3.5, 1, 2.5) superlattice reflection of pure CuGeO$_3$ at $T=4$ K for different magnetic fields. The solid lines are results of the fits as discussed in the text.

FIG. 3. (a) Scans through the (3.5, 1, 2.5) superlattice reflection of pure CuGeO$_3$ at $T=4$ K, $H=12.4$ T on a semilogarithmic scale. (b) Scans through the third-harmonic position of the same reflection at different magnetic fields for $T=4$ K. The solid lines are results of fits as discussed in the text.

tensities and positions were extracted from these data by fitting to Gaussians of width equal to the instrumental resolution. The incommensurability of the third harmonic was constrained to be three times that of the first harmonic. In the region of phase coexistence some intensity at the commensurate position was included in the fit. Only the peak intensities and the incommensurability were fitted. As evidenced by the quality of the fits in Figs. 1 and 3, no other parameters were necessary.

The field dependence of the incommensurability, ΔL, is shown in Fig. 4(a), together with the data for the diluted samples that have reduced transition fields. In Fig. 4, ΔL is measured from the commensurate peak position, that is, $\Delta L=0$ corresponds to the lattice dimerization. The solid line in Fig. 4(a) is the incommensurability calculated by Cross[16] in high magnetic fields for the Heisenberg spin Hamiltonian:

$$\Delta L = \frac{2g\mu_B H}{\pi J_c c}, \tag{1}$$

where $g=2.21$ is the g factor in the magnetic-field direction[13] and c is the spin-chain lattice constant. The theory of Cross takes into account only one harmonic of the lattice modulation in the high-field phase and does not de-
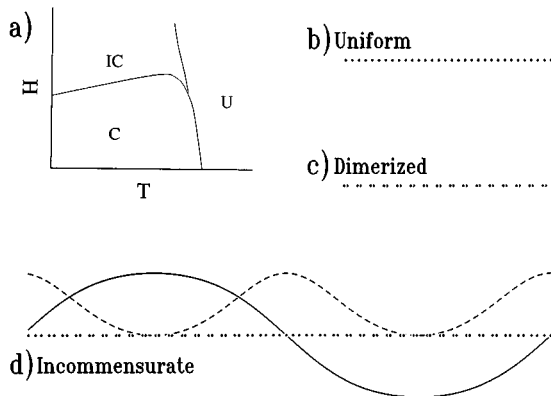

FIG. 2. Magnetic phase diagram (a) and sketches of the positions of the magnetic Cu atoms within the spin chains in the uniform (b), commensurate (c), and incommensurate (d) phases. For clarity the atomic displacements were multiplied by 100. In (d), the solid line shows the amplitude of the lattice distortion of the form of Eq. (4) calculated with the measured parameters for $H=12.7$ T. The dashed line shows the corresponding distribution of the magnetization calculated using an expression given by Buzdin, Kulic, and Tugushev (Ref. 19).
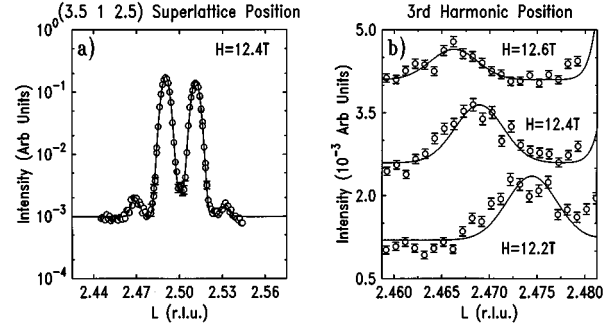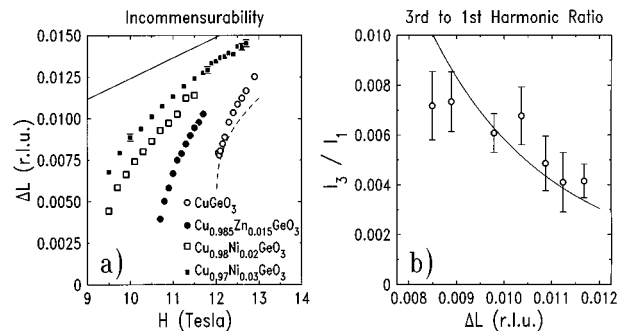

FIG. 4. (a) Magnetic-field dependence of the incommensurability ΔL for pure and diluted CuGeO$_3$. The solid line is the prediction of Eq. (1) for the high-field incommensurability. The dashed line is given by Eq. (2) in the text. (b) Third-to-first-harmonic intensity ratio as a function of the incommensurability ΔL of panel (a). The solid-line is the result of a fit to Eq. (5) in the text.

modulation in the IC phase, we have taken data with high counting statistics. Figure 3(a) shows such a scan at $T=4$ K, $H=12.4$ T on a logarithmic scale. A weak third-harmonic reflection is clearly visible. Scans through the third-harmonic position at different fields are shown in Fig. 3(b). As evident from the figure, the amplitude of the third-harmonic reflection decreases markedly with increasing field. The peak in-

scribe the behavior of the system near the C-IC transition boundary, but the data of Fig. 4(a) from both pure and diluted samples are consistent with an asymptotic approach to this line in high fields.

More recent theories[17–20] have taken all possible harmonics of the fundamental wave vector into account and predict that the lattice modulation has the more complex form of a soliton lattice. As the phase boundary between IC and C phases is approached by lowering the field, the period of the lattice modulation is predicted to smoothly approach the value corresponding to the dimerized lattice. In real space, this translates into a divergence of the intersoliton distance. The data shown in Fig. 4(a) are qualitatively consistent with this behavior, although the divergence of the intersoliton distance does not come to completion as a first-order transition intervenes.[10] Such a weakly first-order transition was in fact predicted by Buzdin, Kulic, and Tugushev[19] who investigated spin-Peierls systems in a magnetic field in the framework of the XY model. According to their calculations, the critical behavior of the incommensurability is given by

$$\Delta L = \frac{\pi \Delta_0}{2 v_s \ln(4/\gamma)}, \qquad (2)$$

where Δ_0 is the zero-field spin excitation gap, $v_s = J_c c$ is the spin-wave velocity for the XY model, and $(H - H_c)/H_c = \gamma^2 \ln(4/\gamma)/2$. As appropriate for CuGeO$_3$, we have substituted the spin-wave velocity for the Heisenberg model, $v_s = \pi J_c c/2$, into Eq. (2). The dashed line in Fig. 4(a) is given by Eq. (2) with $J_c = 10.4$ meV and $\Delta_0 = 2.05$ meV measured by Nishi, Fujita, and Akimitsu[3] at $T = 4$ K, and $H_c = 12$ T. Even with the correct value of v_s, the agreement of the theory with the experimental data is not very close, and further theoretical work is necessary to obtain a satisfactory description of the critical behavior near the C-IC transition.

The intensity ratio of third and first diffraction harmonics, I_3/I_1, is plotted in Fig. 4(b) as a function of the incommensurability of Fig. 4(a). While measuring the position of the first harmonic, (ΔL), provides us with the value of the period of the lattice modulation, the quantity I_3/I_1 parametrizes the shape of the modulation, $u(x)$, where u is the displacement of the magnetic atom at position x along the spin chain from its position in the uniform phase. We write $u(x)$ in terms of its Fourier components, $u(x) = \Sigma_m a_m \sin(m\theta)$, where $\theta = qx$ and q is the momentum transfer along the spin chain reduced to the first Brillouin zone. The intensity I_n of the nth diffraction harmonic is given by

$$I_n \sim \left(\int_0^\pi d\theta \, \sin(n\theta) \sin\left[Q \sum_m a_m \sin(m\theta) \right] \right)^2, \qquad (3)$$

where Q is the total momentum transfer along the spin chain. Even if $u(x)$ is a pure sine wave, $u(x) = \epsilon \sin(qx)$, Eq. (3) shows that higher diffraction harmonics should be present. Specifically, $I_n \sim J_n^2(Q\epsilon)$, where J_n is a Bessel function of the nth order. However, if $Q\epsilon \ll 1$, Eq. (3) simply reduces to the Fourier transform of $u(x)$, and $I_1 \sim (Q\epsilon)^2$, $I_2 = I_3 = \ldots \approx 0$ for a sine wave. Based on a detailed crystallographic study, Hirota et al.[14] reported $\epsilon = 0.0028c$ in the C phase at low temperatures. For the reciprocal-space position studied in our experiment we thus obtain $Q\epsilon = 0.04 \ll 1$, so that I_n is simply

proportional to the square of the Fourier transform of $u(x)$. (We find that to within $\sim 10\%$ the integrated intensity summed over both IC reflections is the same as the integrated intensity of the C reflection, which means that the amplitudes of the C and IC lattice modulations are identical within the experimental error.)

As expected from this argument, the intensity ratio of the third and first diffraction harmonics of Fig. 4 is several orders of magnitude larger than the one corresponding to a sinusoidal lattice modulation in the IC phase. [Equation (3) predicts that $I_3/I_1 \sim 10^{-8}$ in such a case.] Hence the shape of the lattice distortion is more complex and in fact is consistent with theories that predict the existence of a soliton lattice in the IC phase. In the soliton lattice model, the solitons are well separated close to the C-IC transition, and the lattice modulation resembles a square wave with a large harmonic content. Far from the transition the soliton density increases and the solitons overlap more strongly, so that the harmonic content decreases. Also, because of the bond alternation only odd harmonics are relevant for the IC lattice modulation in spin-Peierls systems. All of these qualitative features of the soliton lattice model are observed in the data of Fig. 3.

A functional form that has been widely applied to multisoliton states in one-dimensional systems[21,22] and to the IC phase in spin-Peierls systems in particular[18–20] is

$$u(l) = (-1)^l \epsilon \, \text{sn}\left(\frac{lc}{\Gamma k}, k \right), \qquad (4)$$

where l designates a lattice site, $\text{sn}(x,k)$ is a Jacobi elliptic function of modulus k, and Γ is the soliton half width. The intersoliton distance (half the wavelength of the lattice modulation) is $\pi/\Delta L = 2kK(k)\Gamma$, where K is the complete elliptic integral of the first kind. The Fourier coefficients of $u(l)$ are[23] $a_{2m+1} = [Y^{(2m+1)/2}/(1 - Y^{2m+1})]\epsilon$, where $Y = \exp[-\pi K(\sqrt{1-k^2})/K(k)]$. Following our reasoning above, we can thus write

$$\frac{I_3}{I_1} = \left(\frac{Y}{Y^2 + Y + 1} \right)^2. \qquad (5)$$

This allows us to implicitly express I_3/I_1 as a function of Γ and the measured incommensurability ΔL. The result of a fit of this expression to our data is shown in the solid line of Fig. 4(b). We obtain $\Gamma = (13.6 \pm 0.3)c$, where $c = 2.94$ Å is the lattice constant in the spin-chain direction. In the field range we investigated, Γ is comparable to the intersoliton distance $(\sim 40 - 70c)$, and the solitons therefore overlap significantly. A pictorial rendition of the actual soliton lattice specified by Eq. (4) with the experimentally measured parameters is given in Fig. 2(d).

Expression (5) was derived from Eq. (3), which in turn is based on a continuum approximation for the lattice modulation. As a crosscheck on the validity of this approximation, we have also numerically evaluated the structure factor of the *discrete* lattice described by Eq. (4). The exact ratio I_3/I_1 determined in this manner is in excellent agreement with the approximate expression (5) over the entire field range we investigated.

We can compare our measurement of the soliton width to predictions in the literature. For the (nearest-neighbor) Heisenberg model, Nakano and Fukuyama[17] obtain

$$\Gamma = \frac{\pi J_c c}{2\Delta_0},\qquad(6)$$

where Δ_0 is the zero-field excitation gap. Using $J_c = 10.4$ meV and $\Delta = 2.05$ meV measured by Nishi *et al.*[3] (at $T = 4$ K), we obtain $\Gamma = 8.0c$, significantly lower than the measured value. The measured intensity ratio of third- and first-harmonic reflections is actually *more than a factor of 5* smaller than theoretically predicted.

In principle, the intensities of higher harmonic satellites can be affected by a ''static Debye-Waller factor'' due to pinning-induced randomness in the positions of the solitons. We can get a rough estimate of the amount of disorder necessary to produce such an effect by taking an analytic expression derived by Axe[24] as a guideline. According to Axe, phason disorder gives rise to a Debye-Waller of the form $\exp(-n^2\langle\delta\phi^2\rangle)$ for the intensity of the nth harmonic satellite of an incommensurate structure, where $\langle\delta\phi^2\rangle$ is the mean-square phase fluctuation. Note that this expression is independent of the total momentum Q. We will assume that the impurities (concentration x) act as strong pinning centers, that is, each impurity completely fixes the position of the neighboring soliton, resulting in maximal phason disorder. Each impurity thus shifts the phase of the lattice modulation over a distance of $\sim 2\Gamma/c = 16$ atoms by an amount of order unity, so that $\langle\delta\phi^2\rangle\sim 2\Gamma x/c$. By this argument, the concentration of strong pinning centers needed to reproduce the experimentally observed factor-of-five suppression of the harmonic ratio is of the order of $x\sim 1-2$ %.

While this estimate provides a rough scale for the amount of disorder which would have to be invoked in order to explain our observations, the expression given by Axe was actually derived for thermal phason disorder and rests on some subtle approximations which may or may not be valid for pinning-induced phason disorder. We have thus implemented the above strong pinning model on a computer in order to get a quantitative estimate of the effect of randomness in the position of the solitons on the intensities of the satellite reflections. We have carefully eliminated finite-size effects by directly calculating the structure factors of large systems ($\sim 10^5$ atoms) with randomly placed pinning centers. The result of this calculation is shown in Fig. 5. The predicted and observed intensity ratios of third- and first-harmonic satellites are shown as arrows in the figure. The exact calculation shows that a concentration $x\sim 2.5$% of strong pinning centers is necessary to suppress the ratio to the observed level, in good agreement with the analytical estimate. We have also implemented various other models where, not surprisingly, even more impurities would be necessary to reproduce the observations.

Fortunately, the effects of impurities on the spin-Peierls state in $CuGeO_3$ are very well documented. The highest quality samples synthesized by various different methods invariably undergo the spin-Peierls transition at $T_{SP} = 14.2-14.3$ K. The transition temperature measured on our $CuGeO_3$ sample is 14.3 ± 0.1 K. Both impurities in the CuO_2 chains (Zn, Ni) and Si impurities substituting for Ge
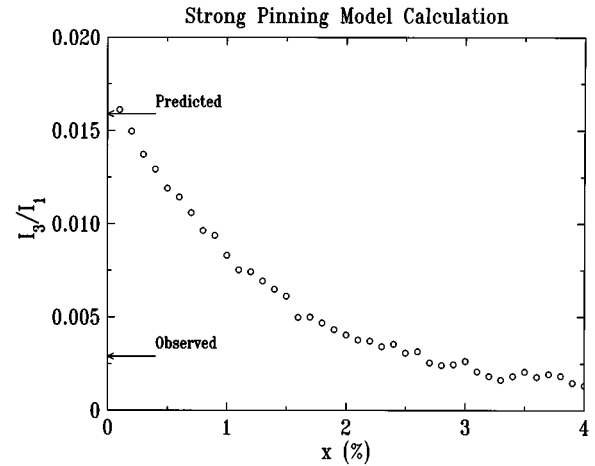

FIG. 5. Dependence of the third-to-first harmonic intensity ratio on the density x of strong pinning centers obtained in a numerical calculation described in the text. The arrows are the predicted and observed ratios, respectively.

suppress T_{SP} very rapidly, at rates of ~ 1.5 and ~ 7 K per percent impurity concentration, respectively. Further, in Sec. IV below we describe direct measurements of the effects of Zn impurities in a dilute concentration of 1.5% on the widths of the lattice modulation in the incommensurate state. In particular, for this concentration of impurities the lattice modulation is only poorly correlated both parallel and transverse to the spin chains, the satellite reflections are severely broadened, and the peak intensities of the satellites are depressed by a factor of 10 compared to those of the pure compound.

At a concentration level of 2.5%, the effects of impurities acting as potential pinning centers are therefore readily recognized. Our direct electron microprobe analysis of the elemental compositions of our crystals is incompatible with impurities at this scale of concentration. Moreover, the optimal zero-field transition temperature and the complete absence of any broadening of the incommensurate Bragg reflections in our pure $CuGeO_3$ samples demonstrate that the impurity concentration must be at least an order of magnitude lower. The corresponding static Debye-Waller factors for the $n=1$ and $n=3$ satellites therefore do not differ appreciably from unity. Similar arguments could be made for soliton pinning by structural imperfections such as dislocations and stacking faults, although little is known about the prevalence of such defects in $CuGeO_3$. In any case, in order to be relevant these would have to have an average separation of about 100 Å (corresponding to a highly disordered crystal), which we regard as unrealistic.

The observed lower-than-predicted intensity ratio of these satellites therefore almost certainly results from a larger-than-predicted soliton width, not from pinning effects. It remains to be seen in how far deviations from the simple nearest-neighbor Heisenberg spin Hamiltonian[15] or the effects of interchain superexchange coupling can account for this discrepancy.

We now turn to the temperature dependence of the lattice modulation. Figure 6 shows scans through the (3.5, 1, 2.5) reflection taken at $H = 12.4$ T at different temperatures. Note the non-monotonic temperature dependence of the C reflection which is absent at low temperatures, then becomes much
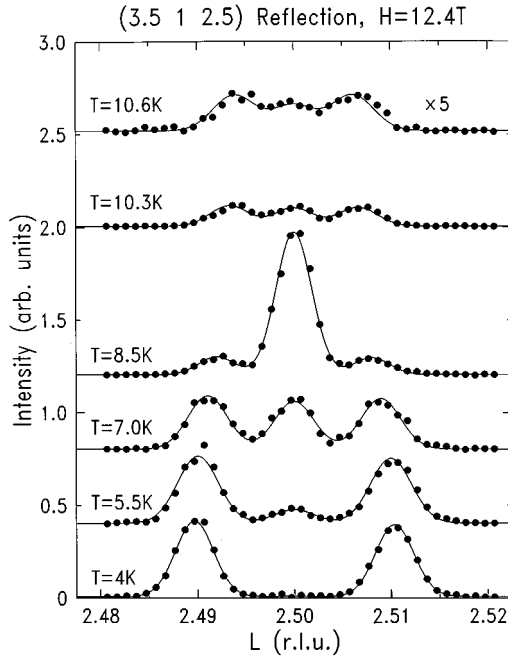
FIG. 6. Scans through the (3.5, 1, 2.5) superlattice reflection at $H=12.4$ T at different temperatures. The solid lines are results of fits, as discussed in the text. The data at $T=10.6$ K were multiplied by 5.
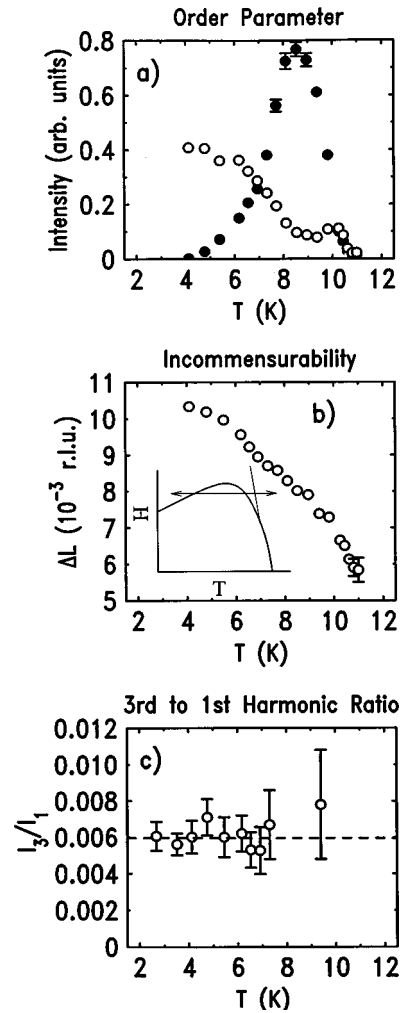

FIG. 7. Temperature dependence of (a) commensurate (filled symbols) and incommensurate (open symbols) peak intensities; (b) the incommensurability, and (c) the third-to-first harmonic intensity ratio for pure $CuGeO_3$ at $H=12.4$ T. The inset in (b) shows the trajectory followed in the H-T phase diagram. Note the reentrancy of the IC phase.

more intense than the IC reflections, and finally dips below the IC reflections again before disappearing in the high-temperature uniform phase. Again, these data were fitted to resolution-limited Gaussians whose intensities are plotted in Fig. 7(a) as a function of temperature. The IC reflections exhibit a reentrant temperature dependence. The intensity minimum of the IC reflections coincides with the intensity maximum of the C reflection, but the IC intensity does not actually go to zero because of the phase coexistence resulting from the first-order nature of the C-IC transition. The reentrancy of the IC phase over a certain field range has been anticipated by theories of the spin-Peierls transition[16,19] [see Fig. 2(a) and inset in Fig. 7]. Our observations are another striking *qualitative* confirmation of these predictions.

Figure 7 also shows the temperature dependence of the incommensurability ΔL and the ratio of third and first harmonics I_3/I_1. ΔL is markedly temperature dependent and has two inflection points at the two consecutive C-IC transitions. By contrast, I_3/I_1 is nearly temperature independent in the temperature range in which we could reliably detect the third harmonic. The C-IC phase boundary terminates in a multicritical (Lifshitz) point. Our experiments near this point have thus far been limited by the small signal intensities and insufficiently accurate temperature control, but improved measurements are currently underway.

IV. $Cu_{1-x}(Zn, Ni)_x GeO_3$

The detailed description of the magnetic phase behavior of the pure compound obtained in the previous section provides a solid basis for an investigation of the microscopic origin of the dramatic effects of impurities on the magnetic phase diagram. We have performed an extensive set of mea-

surements on three diluted samples: $Cu_{0.985}Zn_{0.015}GeO_3$, $Cu_{0.98}Ni_{0.02}GeO_3$, and $Cu_{0.97}Ni_{0.03}GeO_3$. The characterization of these samples is described in Sec. II.

Figure 8 shows a typical set of longitudinal scans (parallel to the spin chains) obtained on the $Cu_{0.985}Zn_{0.015}GeO_3$ crystal, both as a function of field and as a function of temperature. We have taken many such sequences of longitudinal scans for all three samples. In addition, we have also taken analogous sequences in the $(3.5K, K, 0)$ direction transverse to the spin chain direction. As noted above, this direction is almost parallel to the a direction of the crystal lattice. The data were fitted to two equal Lorentzians convoluted with the Gaussian resolution function in the IC phase, and to a single such peak in the C phase. The fitting parameters were the Lorentzian width, the peak intensity and the incommensurability.

Several features are readily apparent from the raw data of Fig. 8: First, the diffraction peaks in the IC phase are substantially broadened, which reflects a loss of translational long-range order. Figure 9 shows the fitted Lorentzian peak
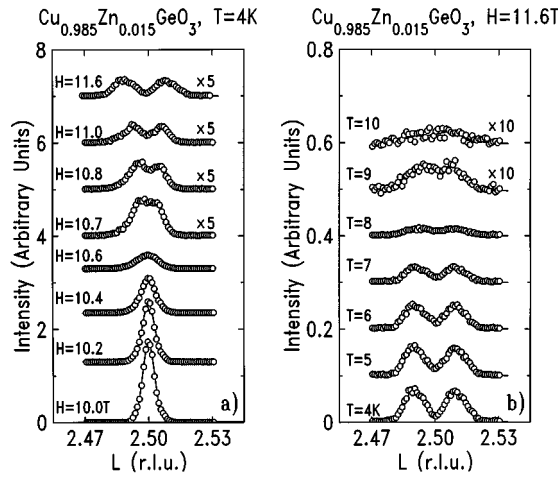
FIG. 8. Scans through (3.5, 1, 2.5) position of $Cu_{0.985}Zn_{0.015}GeO_3$ at (a) constant temperature ($T=4$ K) and (b) constant field ($H=11.6$ T). The solid lines are results of fits as discussed in the text.

FIG. 10. Intensity $I(T)$ of the (3.5, 1, 2.5) superlattice peak for $Cu_{0.97}Ni_{0.03}GeO_3$ at different magnetic fields. The solid lines are results of fits to a quadratic temperature dependence near the maxima of $I(T)$. The data at $H=9$ and 10 T were multiplied by factors of 3 and 4, respectively.

width (half width at half maximum) as a function of field for two samples, $Cu_{0.985}Zn_{0.015}GeO_3$ and $Cu_{0.97}Ni_{0.03}GeO_3$. Both the longitudinal and the transverse widths saturate at high fields. The correlation lengths corresponding to the saturation values of Fig. 9 are $\xi_c=(80\pm8)c$ and $\xi_a=(15\pm2)a$ for $Cu_{0.985}Zn_{0.015}GeO_3$, and $\xi_c=(25\pm5)c$ and $\xi_a=(2.5\pm0.5)a$ for $Cu_{0.97}Ni_{0.03}GeO_3$. The correlation lengths of $Cu_{0.98}Ni_{0.02}GeO_3$ are almost identical to those of $Cu_{0.985}Zn_{0.015}GeO_3$. As shown in the inset of Fig. 11, even the C phase is only short-range ordered for $Cu_{0.97}Ni_{0.03}GeO_3$, whereas no broadening of the C Bragg reflections is observed for the more lightly diluted samples within our resolution. Scans in the b direction are less accurate due to the limited stepping accuracy of our sample rotator. We can nevertheless conclude that $\xi_a \lesssim \xi_b$, which qualitatively mirrors the anisotropy of the zero-field critical fluctuations in pure $CuGeO_3$.[25]

The longitudinal correlation lengths in the IC phase are comparable to the average distance between the impurities in the spin chains. This indicates strong pinning interactions between the impurities and the magnetic solitons. 3% of such
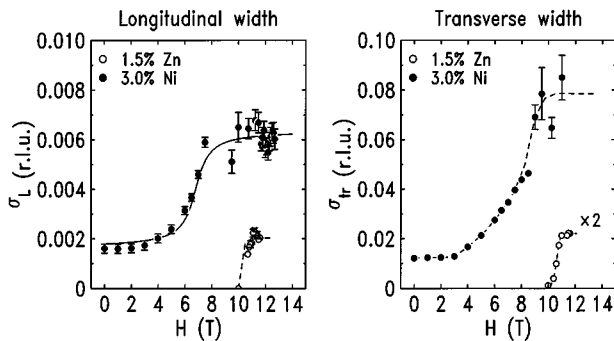

FIG. 9. Magnetic-field dependence of the intrinsic width of the superlattice reflections in the chain direction (σ_l), and perpendicular to it (σ_{tr}) for $Cu_{0.985}Zn_{0.015}GeO_3$ and $Cu_{0.97}Ni_{0.03}GeO_3$ samples at $T=4$ K. The solid line is the result of a fit as discussed in the text. The dashed lines are guides to the eye.

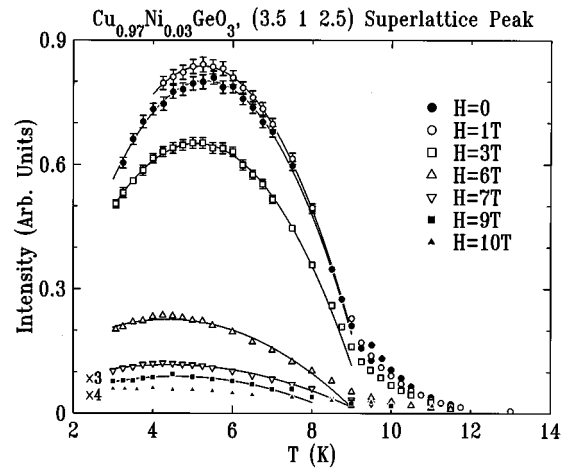impurities are sufficient to reduce the transverse correlation length to only 2.5 lattice spacings, reflecting an almost complete disruption of the transverse spin correlations. As the Bragg reflections in the IC phase are broadened, the peak intensity is reduced. The signal-to-background ratio is thus not large enough to detect third-harmonic satellites for any of the diluted samples. However, the integrated intensity of the superlattice reflections does not change (to within a ~30% experimental uncertainty) in going through the C-IC transition. This implies that the average displacement of the atoms from their positions in the undistorted lattice remains approximately the same in the C and IC phases at a given temperature.

The data of Figs. 8 and 9 differ from those of the pure system (Fig. 1) in another respect. While for pure $CuGeO_3$ the IC wave vector discontinuously jumps to a nonzero value at the C-IC transition signaling a (weakly) first-order transition, there is no sign of such a discontinuity in the diluted samples. Rather, the two broadened IC reflections simply merge as the field is lowered. Over a range of ~0.5 T the peak width narrows continuously and becomes resolution limited in the C phase. In a small field range the peak width cannot be unambiguously extracted from the data as these can be fitted to either a single, broad C peak or to two unresolved, narrower IC peaks. Due to this ambiguity there is a small gap in the fitted peak widths in the vicinity of the C-IC transition (Fig. 9).

The field dependence of the longitudinal and transverse peak widths depicted in Fig. 9 is best described as a disorder-induced broadening of the C-IC transition. Similarly, as shown in the order-parameter curves of Fig. 10, the commensurate-to-uniform transition of $Cu_{0.97}Ni_{0.03}GeO_3$ is also markedly broadened. Such broadening of the zero-field transitions was previously observed in Si-substituted samples[9] and was attributed to an inhomogeneity of the Si content. However, direct measurements on our samples indicate that the macroscopic concentration gradient is less than 0.1%. In view of the dilute impurity concentrations there is also no plausible mechanism for creation of an astatistical

distribution of the impurities on a microscopic or mesoscopic scale.

We propose an alternative mechanism for the broadening of the transitions. Specifically, as the spin chains are split into segments by the impurities, the lifetime of the spin excitations is expected to be limited by finite-size effects. A rough estimate of this lifetime is $\tau = \lambda/v_s$, where $v_s = \pi J_c c/2$ is the spin-wave velocity and λ is the average distance between the impurities. The lifetime limitation is particularly important at the zone center, where it results in a broadening of the spin excitation gap $\Delta_0 \sim 2$ meV. Taking $J_c \simeq 10$ meV and $\lambda \simeq 30c$ for $Cu_{0.97}Ni_{0.03}GeO_3$, the corresponding Lorentzian width of the zone-center spin excitation is $\delta\Delta_0 \simeq 0.25$ meV. Neutron-scattering data indeed suggest that the spin excitations in diluted $CuGeO_3$ are broadened,[4] although poor count rates make a quantitative determination of this effect difficult. Since Δ_0, T_{SP}, and H_c are simply related (for instance, $\Delta_0 = 1.765 T_{SP}$, $\mu_B H_c = 0.75 k_B T_{SP}$ in mean-field theory), we obtain

$$\frac{\delta\Delta_0}{\Delta_0} \sim \frac{\delta T_{SP}}{T_{SP}} \sim \frac{\delta H_c}{H_c} \sim 0.1 \quad (7)$$

for $Cu_{0.97}Ni_{0.03}GeO_3$. A similar estimate for $Cu_{0.985}Zn_{0.015}GeO_3$ yields ~ 0.05 for these ratios.

In order to extract δT_{SP} and δH_c quantitatively from our data, we assume Lorentzian distributions of the transition temperature and field, which follows naturally from a Lorentzian lifetime broadening of the spin excitations. For the longitudinal width of the superlattice reflections at low temperatures we write

$$\sigma_L(H) = \sigma_C + \frac{1}{\pi} \int_0^H dh (\sigma_{IC} - \sigma_C) \frac{\delta H_c}{\delta H_c^2 + (h - H_c)^2}. \quad (8)$$

This allows for two different peak widths σ_C and σ_{IC} in the C and IC phases, as observed and qualitatively explained by the soliton pinning model discussed above. The result of the fit with $\delta H_c = (0.75 \pm 0.25)$ T and $H_c = (7 \pm 0.5)$ T is shown in Fig. 9. The ratio $\delta H_c/H_c$ is thus in good agreement with our estimate in Eq. (7) above. Likewise we write

$$\sigma_L(T) = \sigma_C + \frac{1}{\pi} \int_0^T dt\, \sigma_{x=0}(T - t) \frac{\delta T_{SP}}{\delta T_{SP}^2 + (t - T_{SP})^2} \quad (9)$$

for the temperature dependence of the longitudinal width at low fields (Fig. 11). Following Refs. 25 and 26, we have $\sigma_{x=0} (T - T_{SP}) = \sigma_0[(T - T_{SP})/T_{SP}]^{1/2}$. The best fit was obtained with $\sigma_0 \sim 0.04$ Å^{-1} for $Cu_{0.97}Ni_{0.03}GeO_3$, in the same range as the values of $\sigma_0 \sim 0.15$ Å^{-1} and $\sigma_0 = 0.015$ Å^{-1} reported for pure $CuGeO_3$ by Pouget et al.[25] and Harris et al.,[26] respectively. Figure 11 shows that Eq. (9) with a fitted $\delta T_{SP}/T_{SP} \sim 0.1$ describes the overall temperature dependence of the correlation length quite well, although there are some systematic deviations. Similar analyses have been carried out for the temperature and field dependences of the order parameter and for the more lightly diluted samples, and the results are also qualitatively consistent with our interpretation.

Figure 12 shows the temperature dependences of the incommensurabilities in the $Cu_{0.985}Zn_{0.015}GeO_3$ and

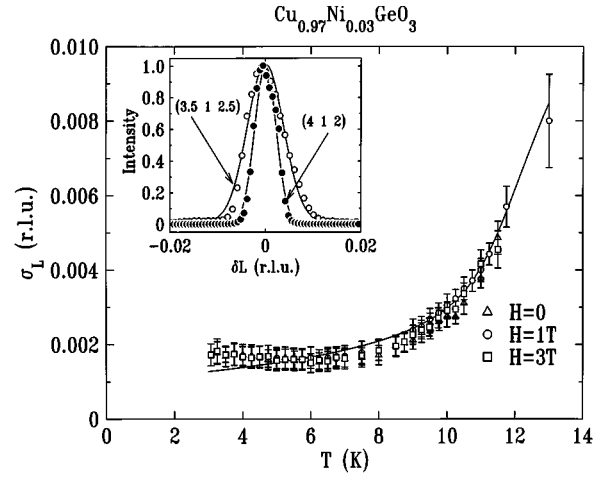FIG. 11. Lorentzian peak width versus temperature for $Cu_{0.97}Ni_{0.03}GeO_3$ for different magnetic fields. The solid line is the result of a fit as described in the text. The inset shows the diffraction profiles of the principal Bragg peak (4,1,2) and the superlattice peak (3.5, 1, 2.5) at $H=0$ and $T=5$ K, scaled to their respective maximum intensities. δL is the deviation from the peak center along the c^* direction.

$Cu_{0.97}Ni_{0.03}GeO_3$ samples at fields just above their respective C-IC transition fields. It is apparent that the strong temperature dependence of the incommensurability in the pure system [Fig. 7(b)] is rapidly diminished upon dilution, such that the incommensurability becomes nearly temperature independent in $Cu_{0.97}Ni_{0.03}GeO_3$. The broadened IC reflections and temperature-independent incommensurability observed in this sample are reminiscent of similar observations in the organic spin-Peierls compound TTF-CuBDT.[27] This suggests that the magnetic phase diagrams of TTF-CuBDT and its derivatives studied extensively in the 1970's (Ref. 2) are strongly affected by disorder.

In accord with previous reports[4–6] we find that the $Cu_{0.97}Ni_{0.03}GeO_3$ sample undergoes a Néel transition at low temperatures. In order to study the transition to the antifer-
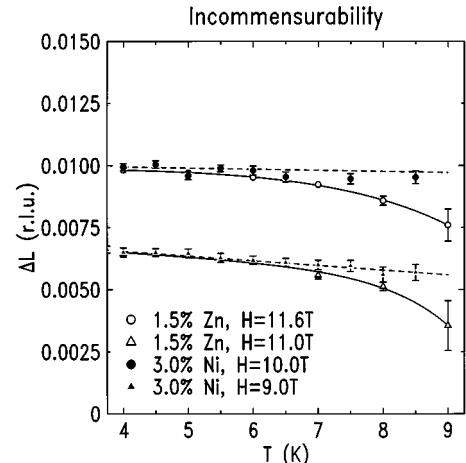
FIG. 12. Incommensurability versus temperature for 1.5% Zn- and 3% Ni-substituted samples at different magnetic fields. The lines are guides to the eye.
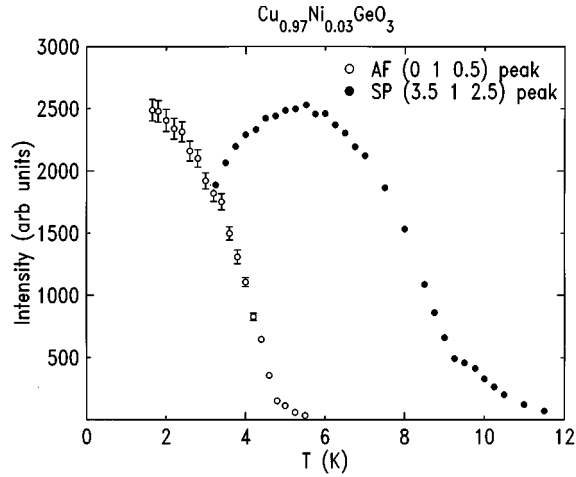
FIG. 13. Temperature dependences of the intensities of the antiferromagnetic (0, 1, 0.5) reflection measured by neutron scattering (open symbols), and of the (3.5, 1, 2.5) structural spin-Peierls reflection (filled symbols, x-ray data) in $Cu_{0.97}Ni_{0.03}GeO_3$.

FIG. 14. Tentative magnetic phase diagram for $Cu_{0.97}Ni_{0.03}GeO_3$ with U (uniform paramagnetic), SP (dimerized spin-Peierls), IC (incommensurate), and AF (antiferromagnetic) phases.

romagnetically ordered state, neutron-scattering measurements were performed on this sample. Figure 13 shows the zero-field temperature dependence of the intensity of the (0, 1, 0.5) magnetic Bragg peak measured by neutron diffraction, along with the spin-Peierls dimerization peak (3.5, 1, 2.5) measured by x-ray diffraction. The Néel transition takes place at $T_N \sim 5$ K, somewhat higher than previously reported Néel temperatures. At the same temperature the spin-Peierls dimerization peak intensity starts to diminish with temperature. Evidently, the onset of the Néel state suppresses the spin-Peierls phase. The two phases coexist over some temperature range below T_N. Similar behavior was observed before in Si-substituted compounds.[9] This implies the formation of separate domains of Néel and spin-Peierls phases. Within our experimental error, the correlation length of the spin-Peierls phase does not show any anomaly at T_N (Fig. 11), which implies that the size of the dimerized domains remains the same at low temperatures.

On a qualitative level, these observations can again be understood in the context of a simple model based on the fact that substitution of Cu by Zn or Ni produces finite-size chain segments. Different behavior is expected for segments containing even and odd numbers of spins: All spins can be accommodated in singlets if the number of spins is even, and such segments therefore naturally continue to undergo the spin-Peierls transition. By contrast, a net unpaired spin exists in segments containing an odd number of spins. It is plausible to assume that the propensity to undergo the spin-Peierls transition is significantly reduced in these segments, and that the Néel state is the ground state under these circumstances. However, alternative models have also been proposed.[28]

Although we did not perform neutron-scattering measurements in magnetic fields, the reduction of the spin-Peierls dimerization peak intensity with the onset of the antiferromagnetic order allows us to determine T_N at various magnetic fields using the data of Fig. 10. The corresponding magnetic phase diagram for the 3% Ni-substituted sample is shown in Fig. 14. The low-temperature, low-field part of the
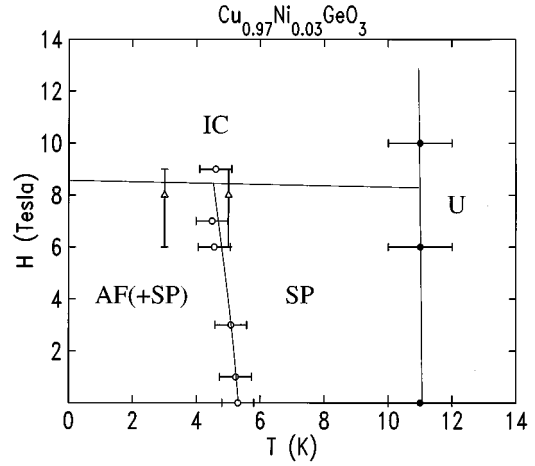
phase diagram contains coexisting spin-Peierls and Néel states. The Néel temperatures at different fields were extracted by fitting the temperature dependence of the (3.5, 1, 2.5) peak intensity to parabolas, as shown in Fig. 10. Large error bars for the transition to the uniform phase arise from the broadened character of these transitions. At fields in excess of the C-IC transition field the intensity of the IC structural Bragg reflections increase monotonically with decreasing temperature. From this we infer that the Néel state is supplanted by the IC modulated phase at high fields. Of course, this should be confirmed by neutron diffraction in high fields.

V. CONCLUSION

In summary, the theoretical concepts developed in the 1970's provide an excellent qualitative description of the magnetic-field-induced C-IC transition in $CuGeO_3$. In particular, we have confirmed the existence of the predicted soliton lattice phase and found that the evolution of the lattice modulation with magnetic field and the shape of the phase boundaries are qualitatively consistent with theoretical predictions. However, as the parameters characterizing the spin excitation spectrum of $CuGeO_3$ are all known to high accuracy, we can go much further and test these theories on a truly quantitative level. Here we found that the currently available theories [all of which are based on a one-dimensional (1D) nearest-neighbor Heisenberg Hamiltonian coupled to 3D phonons] predict neither the soliton density nor the soliton width in the IC phase correctly. Further work is necessary to ascertain whether the origin of these discrepancies lies in an inherent inadequacy of the approximations underlying the work of Refs. 17–20, or whether additional terms in the spin Hamiltonian of $CuGeO_3$ (such as interchain or long-range intrachain exchange interactions) are responsible.

The experiments on the diluted samples demonstrate that (a) the IC phase is extremely sensitive to impurities: the IC Bragg reflections are severely and anisotropically broadened, revealing correlation lengths transverse to the spin chains as

short as 2.5 lattice spacings for $Cu_{0.97}Ni_{0.03}GeO_3$; (b) both the C-uniform and the C-IC transitions are depressed and broadened; and (c) for $Cu_{0.97}Ni_{0.03}GeO_3$ even the C phase does not attain long-range order and is instead replaced by a Néel phase at low temperatures. We were able to account for these phenomena qualitatively by considering the consequences of finite-size effects and soliton pinning. However, many features of the experimental results are still puzzling, and the IC phase and C-IC transition in pure and diluted $CuGeO_3$ remain unique and exciting testing grounds for quantitative descriptions of quasi-1D magnets.

[1] M. Hase, I. Terasaki, and K. Uchinokura, Phys. Rev. Lett. **70**, 3651 (1994).

[2] For a review, see J. W. Bray, L. V. Interrante, I. S. Jacobs, and J. C. Bonner, in *Extended Linear Chain Compounds*, edited by J. C. Miller (Plenum, New York, 1982).

[3] M. Nishi, O. Fujita, and J. Akimitsu, Phys. Rev. B **50**, 6508 (1994); L. P. Regnault, M. Ain, B. Hennion, G. Dhalenne, and A. Revcolevschi, *ibid*. **53**, 5579 (1996).

[4] J.-G. Lussier, S. M. Coad, D. F. McMorrow, and D. McK. Paul, J. Phys. Condens. Matter **7**, L325 (1995).

[5] S. B. Oseroff, S-W. Cheong, B. Aktas, M. F. Hundley, Z. Fisk, and L. W. Rupp, Jr., Phys. Rev. Lett. **74**, 1450 (1995).

[6] M. Hase, N. Koide, K. Manabe, Y. Sasago, K. Uchinokura, and A. Sawa, Physica B **215**, 164 (1995).

[7] M. Hase, I. Terasaki, Y. Sasago, and K. Uchinokura, Phys. Rev. Lett. **71**, 4059 (1993).

[8] J.-P Renard, K. Le Dang, P. Veillet, G. Dhalenne, A. Revcolevschi, and L.-P. Regnault, Europhys. Lett. **30**, 475 (1995).

[9] L. P. Regnault, J. P. Renard, G. Dhalenne, and A. Revcolevschi, Europhys. Lett. **32**, 579 (1995).

[10] V. Kiryukhin and B. Keimer, Phys. Rev. B **52**, R704 (1995).

[11] V. Kiryukhin, B. Keimer, J. P. Hill, and A. Vigliante, Phys. Rev. Lett. **76**, 4608 (1996).

[12] Y. Fagot-Revurat, Y. Horvatic, C. Berthier, P. Ségransan, G. Dhalenne, and A. Revcholevschi (unpublished).

[13] H. Hori, M. Furusawa, S. Sugai, M. Honda, T. Takeuchi, and K. Kindo, Physica B **211**, 180 (1995).

[14] K. Hirota, D. E. Cox, J. E. Lorenzo, G. Shirane, J. M. Tranquada, M. Hase, K. Uchinokura, H. Kojima, Y. Sasago, and I. Tanaka, Phys. Rev. Lett. **73**, 736 (1994).

[15] G. Castilla, S. Chakravarty, and V. J. Emery, Phys. Rev. Lett. **75**, 1823 (1995); J. Riera and A. Dobry, Phys. Rev. B **51**, 16 098 (1995).

[16] M. C. Cross, Phys. Rev. B **20**, 4606 (1979); M. C. Cross and D. S. Fisher, *ibid*. **19**, 402 (1979).

[17] T. Nakano and H. Fukuyama, J. Phys. Soc. Jpn. **49**, 1679 (1980); **50**, 2489 (1981).

[18] B. Horowitz, Phys. Rev. Lett. **48**, 742 (1981).

[19] A. I. Buzdin, M. L. Kulic, and V. V. Tugushev, Solid State Commun. **48**, 483 (1983).

[20] M. Fujita and K. Machida, J. Phys. Soc. Jpn. **53**, 4395 (1984).

[21] E. J. Mele and M. J. Rice, Phys. Rev. B **23**, 5397 (1981); M. Nakahara and K. Maki, *ibid*. **24**, 1045 (1981).

[22] K. Machida and M. Fujita, Phys. Rev. B **30**, 5284 (1984).

[23] I. S. Gradshteyn and I. M. Ryzhik, *Tables of Integrals, Series, and Products* (Academic, New York, 1965), p. 8.146.

[24] J. D. Axe, Phys. Rev. B **21**, 4181 (1980).

[25] J. P. Pouget, L. P. Regnault, M. Ain, B. Hennion, J. P. Renard, P. Veillet, G. Dhalenne, and A. Revcolevschi, Phys. Rev. Lett. **72**, 4037 (1994).

[26] Q. J. Harris, Q. Feng, R. J. Birgeneau, K. Hirota, G. Shirane, M. Hase, and K. Uchinokura, Phys. Rev. B **52**, 15 420 (1995).

[27] V. Kiryukhin, B. Keimer, and D. E. Moncton, Phys. Rev. Lett. **74**, 1669 (1995).

[28] H. Fukuyama, T. Tanimoto, and M. Saito, J. Phys. Soc. Jpn. **65**, 1182 (1996).